ACS APPLIED MATERIALS & INTERFACES

Research Article

www.acsami.org

Hydrophilic Nanowire Modified Polymer Ultrafiltration Membranes with High Water Flux

Yi Feng,[†] Qi Liu,[†] Xiaocheng Lin,[†] Jefferson Zhe Liu,[‡] and Huanting Wang*[,†]

[†]Department of Chemical Engineering and [‡]Department of Mechanical and Aerospace Engineering, Monash University, Clayton, Victoria 3800, Australia

Supporting Information

ABSTRACT: Germanate nanowires/nanorods with different lengths were synthesized and used as additives for the fabrication of polymer composite membranes for high-flux water filtration. We for the first time demonstrated that at a small nanowire/nanorod loading (e.g., <0.5 wt % on the basis of poly(ether sulfone)), the length of germinate nanowires was a key parameter in determining their migration and diffusion in the polymer solution, and thus affecting polymer precipitation in the membrane formation process. In particular, short $Ca_2Ge_7O_{16}$ nanowires with an average length of 138.7 nm and an average diameter of 12.7 nm, and Zn_2GeO_4 nanorods with an average length of 400 nm and an average diameter of 18.7 nm quickly diffused out of the membrane, leading to a higher pore density on the active layer in comparison with the pristine membranes. The addition of short $Ca_2Ge_7O_{16}$ nanowires resulted in greater pore sizes than the addition of Zn_2GeO_4 nanorods because the out-diffusion of the former was faster than that of the latter. In contrast, the addition of long $Ca_2Ge_7O_{16}$ nanowires with lengths of several tens to hundreds of micrometers and an average of 27.3 nm was not effective in promoting the pore formation because of partial embedment of nanowires. Poly(ether sulfone) composite membranes prepared by adding a small amount of Zn_2GeO_4 nanorods exhibited dramatically enhanced water permeation without losing rejection property. For example, the poly(ether sulfone) (PES) composite membrane prepared with 0.3 wt % Zn_2GeO_4 nanorods exhibited the highest flux, 1294.5 LMH, which was 3.5 times of the pristine (PES) membrane (384.2 LMH). Our work provides a new strategy for developing high-performance ultrafiltration membranes for practical industrial filtration applications.

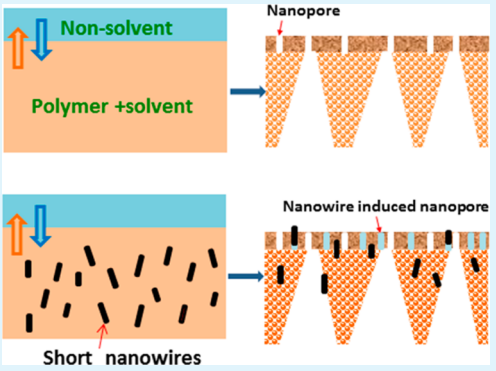

KEYWORDS: *ultrafiltration membranes, polymer, germanate nanowires, high flux, nanoporous structure*

1. INTRODUCTION

Nanoporous membranes with a pore size range of 2−100 nm are classified as ultrafiltration (UF) membranes and used extensively in various processes such as water purification and treatment and pharmaceutical production to remove suspended nanoparticulates, bacteria, macromolecules, etc.[1−5] To date, many polymers such as cellulose acetate (CA), polysulfone (PS), poly(ether sulfone) (PES), polyacrylonitrile (PAN), and bromomethylated poly(phenylene oxide) (BPPO) have been used to produce ultrafiltration membranes with an asymmetrically porous structure via a nonsolvent induced phase inversion method.[6−10] But the current polymer membranes exhibit low water flux, and thus the development of high-performance ultrafiltration membranes is highly desirable to improve the filtration efficiency and meet the ever-growing industrial and environmental requirements.

To improve membrane performance, additives such as organic water-soluble polymers or inorganic materials have been incorporated into polymeric UF membranes to tailor the nanoporous structure.[11−13] Some improvement in water permeability has been achieved by the incorporation of additives such as polyvinylpyrrolidone (PVP), poly(ethylene glycol) (PEG), polyaniline nanorods, and carbon nanotubes (CNTs) via the pore-forming effect and/or the out-diffusion effect of additive.[14−18] However, such water flux improvement is usually accompanied by the great decrease of rejection, hindering their practical applications.[19,20] There have been many studies attempting to minimize the reduction of rejection while achieving fast water permeation. In general, the rejection can be maintained by improving the compatibility between the additive and the polymer, avoiding the agglomeration of the additives and/or increasing the viscosity of casting solution.[21−23] However, the water permeability can be improved only slightly or even decreased compared with the pristine membrane. Therefore, it remains a significant challenge to improve the permeability of membranes while maintaining or even improving the rejection property.[24]

In this work, germanate nanowires with different lengths were prepared as additives for preparation of polymer membranes with enhanced water flux at similar rejections.

Received: August 2, 2014
Accepted: October 12, 2014
Published: October 12, 2014

   dx.doi.org/10.1021/am505157w | ACS Appl. Mater. Interfaces 2014, 6, 19161−19167

The reasons for choosing germinate nanowires are (1) germanate nanowires have high affinity with water;[25,26] (2) germanate nanowires can be well-dispersed and chemically stable in solvent; and (3) germanate nanowires have good surface smoothness, and are not compatible with hydrophobic polymer membrane material. As a commonly used membrane material, poly(ether sulfone) (PES) was chosen to prepare composite UF membranes using the phase inversion method.[27] The germanate nanowires/nanowires and composite membranes were characterized, and the mechanisms for membrane performance enhancement was discussed.

2. MATERIALS AND METHODS

2.1. Chemicals. The chemicals were used as received. They included Ca $(NO_3)_2{\cdot}4H_2O$ (purity ≥99%, Merck KCaA, Germany), CH_3COONa (purity ≥99%, Merck KCaA, Germany), GeO_2 (purity ≥99.99%, trace metals basis, Sigma-Aldrich, Australia), $N_2H_4{\cdot}H_2O$ (65%N_2H_4, Sigma-Aldrich, Australia), $Zn(CH_3COO)_2$ (purity ≥99.99%, Sigma-Aldrich, Australia), tetramethylammonium hydroxide solution (TMAH) (25 wt % tetramethylammonium in H_2O, Sigma-Aldrich, Australia), poly(ether sulfone) (PES, Ultrason E6020P, 51 kDa, BASF, Germany), 1-Methyl-2-pyrrolidone (NMP) (purity ≥99%, Sigma-Aldrich, Australia), poly(ethylene oxide) (PEG) (with molecular weight of 35 kDa, 100 kDa and 200 kDa, Sigma-Aldrich, Australia), ethylene glycol (purity ≥99%, Sigma-Aldrich, Australia), and glycerol (purity ≥99%, Sigma-Aldrich, Australia).

2.2. Sample Preparation. In the synthesis of long $Ca_2Ge_7O_{16}$ nanowires, 1 mmol of Ca $(NO_3)_2{\cdot}4H_2O$, 2 mmol of CH_3COONa and 1 mmol of GeO_2 were added to 15 mL of deionized (DI) water. The mixture was stirred for 30 min and then transferred to a Teflon-lined autoclave. The hydrothermal synthesis was performed at 180 °C for 24 h, followed by natural cooling to room temperature. The product was collected by centrifugation, washed thoroughly with water and ethanol, and then dried at 70 °C in an oven. For the synthesis of short $Ca_2Ge_7O_{16}$nanowires, similar procedures were taken except that 1 mL of $N_2H_4{\cdot}H_2O$ was added into the autoclave and stirred for another 30 min before the hydrothermal treatment.

For the synthesis of Zn_2GeO_4 nanorods, 2.5 mmol of GeO_2 and 5 mmol of Zn $(CH_3COO)_2$ were added into15 mL of TMAH hydroxide solution. The mixture was stirred for 30 min and then transferred to a Teflon-lined autoclave. The remaining steps were the same as the synthesis of long $Ca_2Ge_7O_{16}$ nanowires.

The PES membrane and germanate nanowire/PES composite membranes were prepared via the nonsolvent induced phase inversion method at room temperature.[5,28] The casting solutions were prepared by ultrasonicating nanowires in 17 g of NMP for at least 30 min using a Brason B1510 ultrasonic cleaner (maximum 80 W, Unisonics, Australia), followed by dissolving 3 g of PES to yield 15 wt % PES solution. The amount of nanowires was varied as 0, 0.3, 0.5, and 1.0 wt % on the basis of the PES weight (0, 0.045, 0.075, and 0.15 wt % on the basis of the total weight of PES and NMP), and the resulting membrane samples, the pristine PES membrane, long $Ca_2Ge_7O_{16}$ nanowire/PES composite membranes, short $Ca_2Ge_7O_{16}$ nanowire/PES composite membranes and Zn_2GeO_4nanorod/PES composite membranes, were denoted the pristine, Ca long-X and Ca short-X and Zn-X respectively, where the X indicated the nanowire loading on the basis of PES amount. The casting solutions were stirred for 1 day and kept static for degassing overnight. The solution was then cast onto a clean glass plate using a casting knife (Gardco, USA) with a 150 μm air gap and then immersed into a water bath immediately. After complete coagulation, the membranes were stored in DI water until use.

2.3. Characterization. *2.3.1. XRD, SEM and Contact Angle.* The products of nanowires were characterized using X-ray diffraction (XRD, Miniflex 600, Rigaku, Japan) and scanning electron microscopy (Nova Nano SEM, FEI Company, USA).The cross-sections of membranes were prepared by fracturing membranes in liquid nitrogen and then examined using scanning electron microscopy (Nova Nano SEM, FEI company, USA); the top surface of membranes was characterized using scanning electron microscopy (Magellan SEM, FEI company, USA), and the surface pore size and surface pore size distribution were determined using a NanoMeasurer 1.2 software (Fudan University, China) based on the SEM images of top surface. All the SEM work was performed at an accelerating voltage of 5 kV with secondary electron (SE) detector and all samples were coated with Pt. The hydrophilicity of membrane top surface was characterized using contact angle measurement (Video based optical contact angle measuring instrument, OCA-15EC, Dataphysics, Germany) and each sample was tested at least five times to obtain the average contact angle. The surface energy was calculated from the contact angle values of different solvents (DI water, glycerol and ethylene glycol) using the SCA 21 software (included in OCA 15 EC package) via the Owens, Wendt, Rabel & Kälble (WORK) method. The porosity of membrane was determined by the mass loss of wet membranes after drying.

To observe the surface aggregation of nanowires on the top surface, liquid nitrogen was used to "freeze" the phase inversion process. After casting the solution onto the glass plate and immersing into water within a few seconds, the membrane with 0.5 wt % nanowires/nanorods was quickly taken out and then put into liquid nitrogen to stop the phase inversion process. The top surface of the resultant membrane was characterized using scanning electron microscopy (Magellan SEM, FEI company, USA).

2.3.2. Permeation and Molecular Weight Cutoff. The flux of membranes was measured using a dead end cell (HP4750 Stirred Cell, Sterlitech, USA).[29] The double deionized (DDI) water was added in the cell and the feed pressure was controlled by using a nitrogen gas cylinder. The permeate water was accumulated on a beaker sitting on top of an electronic balance and its mass change was automatically recorded. During the flux test, 150 kPa was used to precompact membrane for at least 30 min until the flux became stable and then the flux was tested and recorded at the pressure of 100 kPa. For each batch, at least five membranes were tested. Rejection test was performed using PEG with the molecular weight of 35, 100, and 200 kDa. The rejection rate was obtained by measuring the organic carbon content in the permeate and feed solution by a total organic carbon analyzer (TOC-LCSH/CSN, Shimadzu, Japan).

2.3.3. Flux Modeling. The theoretical flux was calculated based on the Hagen−Poiseuille model:[30]

$$J' = N\pi {d_p}^4 \Delta P/128\mu l \tag{1}$$

where J' is the theoretical flux, N is the pore density and was determined by counting the number of pores on high-resolution SEM images of the top surface of membranes, ΔP is the pressure drop across the membrane (100 kPa in this study), μ is the viscosity of DDI water at room temperature (0.001 Pa s), and l is the thickness of the skin layer (100 nm) measured from the cross-section of membranes and d_p is the diameter of the nanochannel and in this study is defined as the average surface pore diameter calculated from the molecular weight cutoff values of PEG[31]

$$d_p = 0.262\mathrm{MW}^{0.5} - 0.3[\text{Å}] \tag{2}$$

where MW is the molecular weight cutoff values of PEG.

It should be noted that the theoretical flux was calculated under the assumptions: (1) all the surface pores run through the whole skin layer with a constant diameter and (2) no velocity at the surface of pores was considered. For a flow with a nonzero velocity at the surface, the slip length is considered and calculated based on the following equation

$$J = (1 + L_s/d_p)*(\mathrm{N}\pi {d_p}^4 \Delta \mathrm{P}/128\mu l) \tag{3}$$

$$J = (1 + L_s/d_p)*J' \tag{4}$$

where L_s is the slip length and J is the actual flux obtained from flux test.

3. RESULTS AND DISCUSSION

Figure 1a, b shows the SEM images of the as-synthesized long $Ca_2Ge_7O_{16}$ nanowires with lengths in the range of several tens

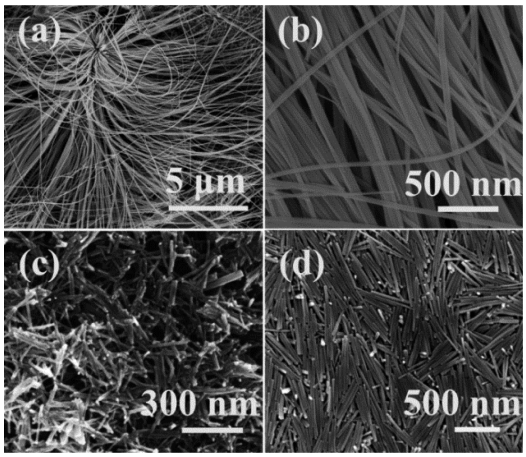

Figure 1. SEM images of (a, b) long $Ca_2Ge_7O_{16}$nanowires,(c) short $Ca_2Ge_7O_{16}$nanowires, and (d) Zn_2GeO_4 nanorods.

to hundreds of micrometers and smooth surface. The typical diameters of the nanowires are in the range of 20−50 nm (the average diameter is 27.3 nm). Figure 1**c** shows the SEM images of modified $Ca_2Ge_7O_{16}$ nanowires. They have an average length of 138.7 nm and an average diameter of 12.7 nm. These modified short $Ca_2Ge_7O_{16}$ nanowires with a broad length range were prepared from long $Ca_2Ge_7O_{16}$ nanowires. By contrast, all Zn_2GeO_4nanorods have a similar length of around 400 nm and an average diameter of 18.7 nm (Figure 1d). The XRD peaks of long nanowires (Figure 1a) and nanorods (Figure 1d) can be indexed to the orthorhombic phase of $Ca_2Ge_7O_{16}$ (JCPDS Card No. 34−0286) and Zn_2GeO_4 (JCPDS Card No.11−0687), respectively (Figure 2). No other phase was observed in

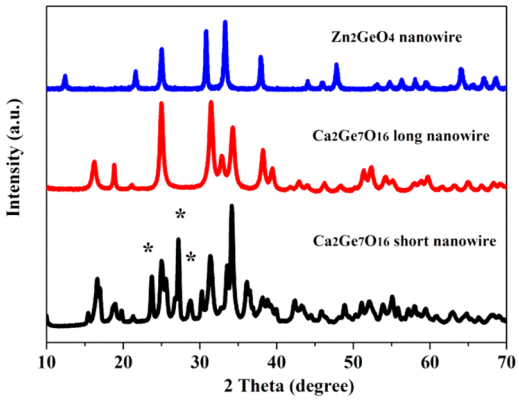

Figure 2. XRD patterns of long and short $Ca_2Ge_7O_{16}$ nanowires and Zn_2GeO_4 nanorods.

these two samples, and this indicates the high purity of as-synthesized samples. However, for the modified short nanowires (Figure 1c), apart from the $Ca_2Ge_7O_{16}$ phase, $CaGeO_3$ phase was observed, as indicated by stars in Figure 2. But the valence state of each element in the short nanowires was the same as that in long nanowires. All three nanowires were well dispersed and chemically stable in NMP, as shown in Figure S1 in the Supporting Information. The viscosity measurement confirmed that the incorporation of germanate nanowires only slightly increased the viscosity of the casting solution. For example, the viscosity was only increased by approximately 0.05 Pa·s with 1.0 wt % nanowire loading (see Figure S2 in the Supporting Information).

The SEM images of top surface of all membranes are shown in Figures S3 and S4 in the Supporting Information. The surface pore density and surface pore size distribution were determined on the basis of the SEM images. From Figure 3a, it is obvious that the pore density of Ca short-X and Zn-X sample is greater than that of Ca long-X sample. This means that more surface pores were created with the addition of short nanowires such as short $Ca_2Ge_7O_{16}$ nanowires and Zn_2GeO_4 nanorods compared with the long $Ca_2Ge_7O_{16}$ nanowires. Moreover, for the Ca short-X and Zn-X samples, the number of large pores (larger than 9 nm) is greater than that of Ca long-X sample. At the same nanowire loading (e.g., 0.3 wt %), the percentage of pores with pore size larger than 9 nm is 70, 45, and 25% for Ca short-0.3 sample, Zn-0.3 sample and Ca long-0.3 sample, respectively (Figure 3b). The greater sizes of the nanopores created by Ca short-0.3 nanowires, compared with Zn-0.3 nanorods, can be explained by faster out-diffusion of shorter Ca short-0.3 nanowires (138.7 nm) companied by quicker precipitation of polymer. Note that when the amount of short $Ca_2Ge_7O_{16}$ nanowires is increased to 0.5%, the pore size of the active layer is not further enlarged. However, the increase in pore density on the top surface of the membrane prepared by adding the long nanowires (Ca long-X sample) is less significant compared with the membranes with short nanowires/nanorods. The pore density values for the active layer for typical membranes are listed in Table 1.

For the cross section of membranes, a typical asymmetrical porous structure composed of a thin selective active layer and a thick macroporous supporting layer is observed (see Figure S5 in the Supporting Information). The thickness of the active layer of the pristine and the composite membranes is approximately 100 nm and no big change in pore structure is observed in composite membranes in comparison with the pristine membranes. Furthermore, the porosity of all composite membranes is in the range of 75−80%, which is similar to the pristine membrane (78%). Therefore, the addition of germanate nanowires has little influence on the porosity and the microstructure of the support layer.

The contact angle results are shown in Figure 3**c**. It can be seen that the contact angle decreases from 72 to 64° as the long $Ca_2Ge_7O_{16}$ nanowire loading or Zn_2GeO_4 nanorod loading increases from 0 to 1.0 wt %. In contrast, the contact angle of Ca short-X top surface is lower than that of Ca long-X samples and Zn-X samples at the same nanowire loading, and this is more obvious at high nanowire loading. For example, the contact angle of the top surface of Ca short-1.0 sample is 54.6°, which is 10° lower than that of Ca long-1.0 (64.2°) and Zn-1.0 sample (64.8°). Compared with the PES polymer, germanate nanowires have higher surface energy and the polar component dominates in the total surface energy (Figure 3d). Therefore, these hydrophilic nanowires preferentially migrate to the interface between membrane and nonsolvent (water) in the membrane formation process. As a result, lower contact angle was obtained in composite membranes as compared with the pristine PES membrane. However, for nanowires with short lengths, the migration to the surface occurs more easily, whereas long nanowires may become trapped on their way out.

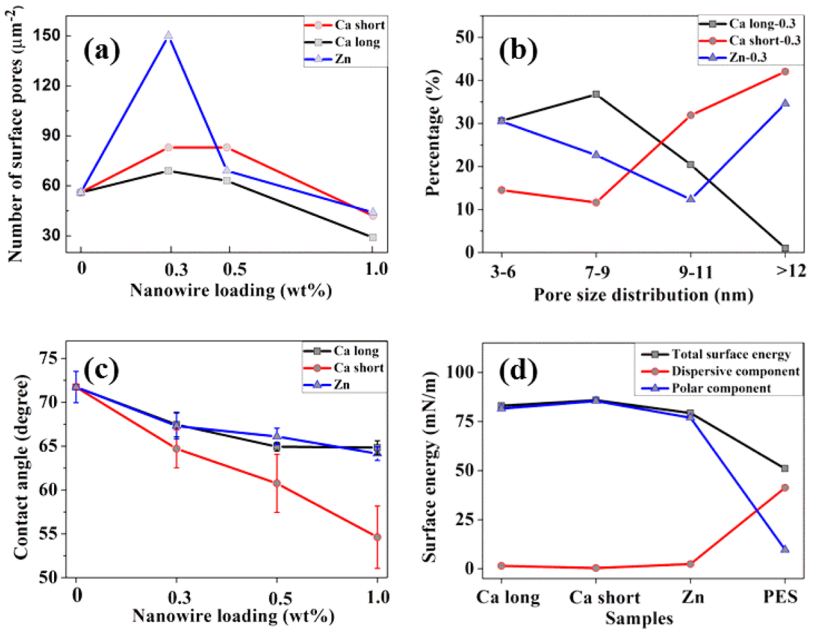

Figure 3. (a) Surface pore density of samples at different nanowire loadings, (b) surface pore size distribution of 0.3 wt % nanowire/PES composite membranes, (c) contact angle of the top surface of samples at different nanowire loadings, and (d) surface energy of long and short $Ca_2Ge_7O_{16}$ nanowires, Zn_2GeO_4 nanorods, and PES.

Table 1. Theoretical Flux and Actual Flux of the Pristine PES Membrane and Composite Membranes[a]

sample	pore size d_p (nm)	pore density N (μm^{-2})	theoretical flux J' (LMH)	actual flux J (LMH)	slip length L_s (nm)
pristine	16.86	56	399.8	384.2	
Ca long-0.3 (>several tens of micrometers long)	16.27	69	427.2	889.4	17.60
Ca short-0.5 (138.7 nm long)	23.50	83	2236.4	1140.8	
Zn-0.3 (400 nm long)	15.75	150	815.5	1294.5	9.25

[a]The pore density data for the membrane active layers was obtained from the SEM images using a NanoMeasurer 1.2 software, and the pore size was calculated from the molecular weight cutoff of PEG.

Therefore, the top surface of Ca short-X sample is more hydrophilic than the other membranes and this is more obvious at a high nanowire loading.

The effect of nanowire length on its out-diffusion process from the polymer was evidenced by SEM studies. The long $Ca_2Ge_7O_{16}$ nanowires were observed either partly "entrapped" on the top of surface (Figure 4a), or in the wall of polymer-lean region (pores) in the support layer (Figure 4b). The long nanowires hindered the movement and the migration of nanowires to the top surface and the polymer-lean region inside polymer during the phase inversion process; therefore only a small portion of long nanowires diffused out of the polymer. By contrast, short $Ca_2Ge_7O_{16}$ nanowires and Zn_2GeO_4 nanorods were observed loosely attached on the top surface of polymer wall, confirming that more short nanowires/nanorods diffused out.

To further investigate the migration of nanowires/nanorods in the fast demixing of solvent and nonsolvent, liquid nitrogen was used to "freeze" the phase inversion process after the cast polymer solution was immersed into water within a few

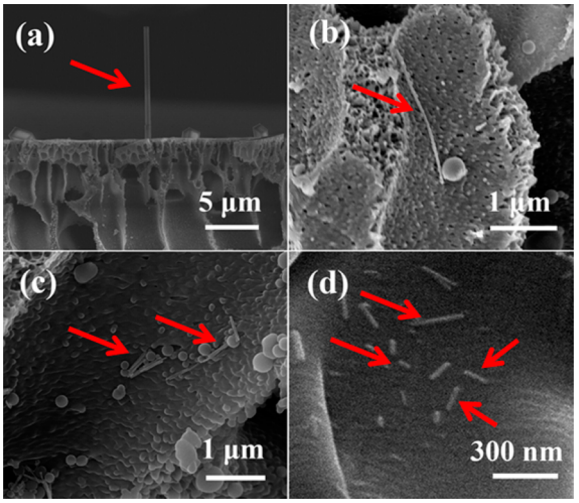

Figure 4. SEM images of nanowires inside the polymer: (a, b) long $Ca_2Ge_7O_{16}$ nanowires, (c) Zn_2GeO_4 nanorods, and (d) short $Ca_2Ge_7O_{16}$ nanowires. The arrows in the figure indicate the location of nanowires and the SEM images are the cross-section of composite membranes.

seconds. More short $Ca_2Ge_7O_{16}$ nanowires were observed on the top surface of the resultant membrane than the long $Ca_2Ge_7O_{16}$ nanowires and the Zn_2GeO_4 nanorods (larger than short $Ca_2Ge_7O_{16}$), as shown in Figure 5. Moreover, most of short $Ca_2Ge_7O_{16}$ nanowires were loosely attached onto the top surface and some of nanowires were agglomerated with gaps between the nanowire agglomerates and the surrounding polymer, which indicated the strong diffusion of short nanowires from the polymer (Figure 5d). In contrast, many long $Ca_2Ge_7O_{16}$ nanowires (Figure 5a, b) and Zn_2GeO_4 nanorods (Figure 5c) were partly buried inside the polymer and tightly bonded with polymer. Note that at the same loading of nanowires/nanorods (0.5 wt %), the number of long $Ca_2Ge_7O_{16}$ nanowires is much smaller than that of short

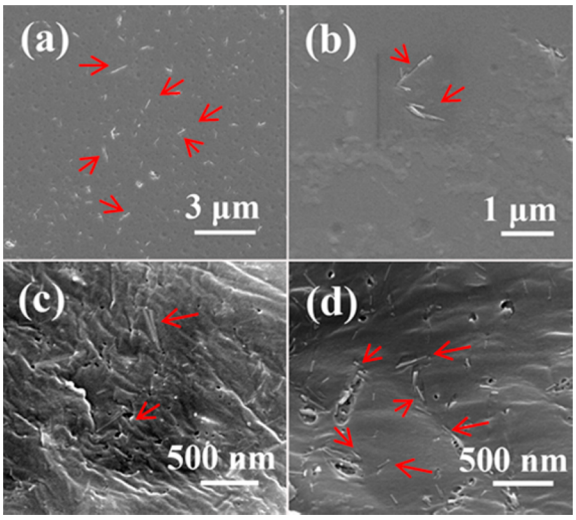

Figure 5. SEM images of nanowires on the top surface of composite membranes: (a, b) long $Ca_2Ge_7O_{16}$ nanowires, (c) Zn_2GeO_4nanorods, and (d) short $Ca_2Ge_7O_{16}$ nanowires. The arrows in the figure indicate the location of nanowires and the membranes were made by freezing the phase inversion process using liquid nitrogen within a few seconds after immersion in a coagulant.

$Ca_2Ge_7O_{16}$ nanowires and Zn_2GeO_4 nanorods, and the number of Zn_2GeO_4 nanorods is smaller than that of short $Ca_2Ge_7O_{16}$ nanowires due to different lengths (assuming they have a similar density). This explains that more short $Ca_2Ge_7O_{16}$ nanowires were observed on the polymer surface. Given partial entrapment of long $Ca_2Ge_7O_{16}$ nanowires and Zn_2GeO_4 nanorods, it is reasonable to conclude that, the length of germanate nanowires appears to be a key factor in affecting their movement in the phase inversion process, and the shorter nanowires are more likely to migrate to the top surface of membranes and even leave the polymer matrix during the fast membrane formation process.

The water fluxes of the pristine and composite membranes are shown in Figure 6. The pristine PES membrane has a flux of

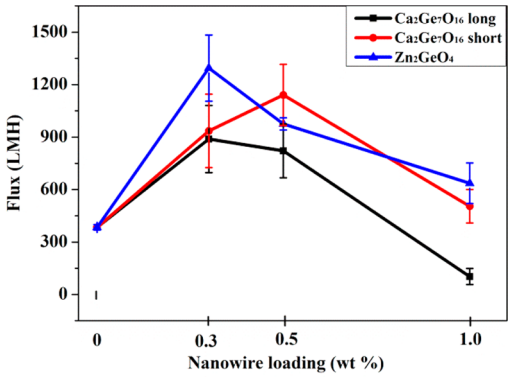

Figure 6. Water flux of the pristine and composite membranes with different loading of nanowires/nanorods.

384.2 l m^{-2} h^{-1} (LMH), whereas the membranes with 0.3 wt % long $Ca_2Ge_7O_{16}$ nanowires, 0.5 wt % short $Ca_2Ge_7O_{16}$ nanowires, and 0.3 wt % Zn_2GeO_4nanorods exhibit greatly enhanced fluxes, 889.4 LMH, 1140.8 LMH, and 1294.5 LMH, respectively. However, the flux decreases with further increasing the nanowire loading up to 1 wt %. The flux drop of Ca long-X sample is the highest; the flux declines to around 100 LMH for 1 wt % $Ca_2Ge_7O_{16}$ nanowire loading, whereas the flux only decreases to around 600 LMH for the Ca short-1.0 and Zn-1.0 sample.

As stated earlier, the porosity of the membranes and the microstructure of support layer of the composite membrane are similar to the pristine membrane, whereas there is noticeable pore structure change in the active layer. Therefore, the active layer (skin layer) plays a dominant role in controlling the water flux of membranes, and the flux improvement in composite membranes should be mainly attributed to the microstructure change of the active layer.

To further investigate the influence of the pore structure change resulting from the out-diffusion of nanowires with different lengths on the flux enhancement, we calculated the theoretical flux based on nanoporous structure of the active layer of the pristine membrane and the composite membranes using the Hagen−Poiseuille model and compared the theoretical flux values with the experimental values, as shown in Table1. The theoretical flux of the pristine membrane is in good agreement with the actual flux. However, for the short $Ca_2Ge_7O_{16}$ nanowire/PES composite membrane, the theoretical flux is much greater than the actual value (almost twice actual flux). A possible reason is that some of the pores created by the out-diffusion of short nanowires are dead-ended and do not run through the whole thickness of skin layer (the Hagen−Poiseuille model is based on the hypothesis that all pores run through the whole layer with a constant diameter); therefore, the limited pore interconnectivity may hinder further flux improvement despite the fact that Ca short-0.5 sample has larger surface pore size and higher pore density than the pristine membrane. In contrast, the theoretical flux of Ca long-0.3 and Zn-0.3 samples is lower than the experimental flux. For a flow with a nonzero velocity at the surface, slip length (L_s) is often used as a quantitative measure to characterize the flow resistance of a slip flow in nanochannels. High slip length value means lower flow resistance, thus higher flux value. Compared to the Zn_2GeO_4 nanorods (average length: 400 nm), the long $Ca_2Ge_7O_{16}$ nanowires have the length of tens of microns; therefore the pores created by the out-diffusion of long $Ca_2Ge_7O_{16}$ nanowires may be better interconnected compared with the pores in Zn-X samples. In sum, the pore size, pore density and pore connectivity/resistance are responsible for the flux change of our membranes and the flux enhancement obtained in composite membranes can be attributed to the larger pore size, higher pore density, and/or the lower flow resistance (improvement of pore interconnectivity).

Despite the water flux enhancement for Ca short-X samples, the rejection was greatly decreased, as shown in Figure 7 and Figure S6 in the Supporting Information. The molecular weight cutoff (MWCO) refers to the lowest molecular weight solute in which 90% of the solute is retained by the membrane. In our work, polyethylene glycol (PEG) with different molecular weight was used to characterize the pore size and rejection rate of membranes. The MWCO values for Ca short-X samples were around 200 kDa while the MWCO of the pristine PES membrane was around 100 kDa, indicating that larger pores were created in the active layer of membrane by adding short $Ca_2Ge_7O_{16}$ nanowires. For Ca long-X and Zn-X samples, the rejection rate for 100 kDa PEG slightly increased and the MWCO slightly decreased. This suggested that the rejection property of Ca long-X samples and Zn-X samples was almost the same or even slightly improved in comparison with the

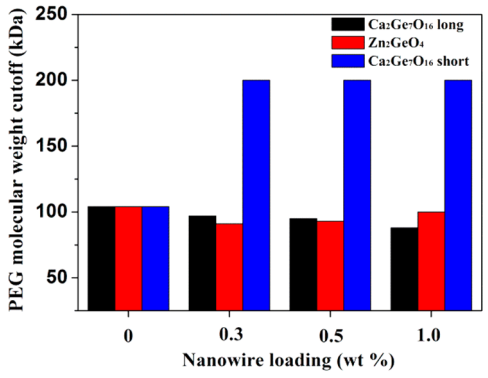

Figure 7. Molecular weight cutoff of the pristine membrane and composite membranes.

pristine PES membrane. Therefore, this again confirms that the length of nanowires plays an important role in determining the pore size in the active layer. Generally, the shorter the nanowires, the larger the average surface pore size; thus higher MWCO or lower rejection was obtained.

As discussed above, short $Ca_2Ge_7O_{16}$ nanowires were much more easily to migrate to the top surface and then diffuse out from the polymer than the other two nanowires/nanorods with greater lengths. Therefore, more pores were created in the active layer resulting from the out-diffusion of nanowires. However, the short nanowires tend to agglomerate on the top surface of membrane during the phase inversion process (Figure 5), increasing the surface pore sizes. As a result, the flux was enhanced but at the sacrifice of rejection. In contrast, the long $Ca_2Ge_7O_{16}$ nanowires became trapped during the migration to the top surface and the diffusion process of nanowires from polymer was hindered (Figure 5). Thus, smaller average surface pore size was obtained but at the same time, the number of surface pores greatly decreased; therefore, the improvement of flux was not as high as that of the composite membranes with short nanowires despite the fact that the rejection was maintained.

Zn_2GeO_4 nanorods had the average length of 400 nm and the separation tendency between the nanorods and PES was moderate. Therefore, the number of surface pores was greatly increased without the enlargement of the pore size. Moreover, it worth noting that in our study the addition of only 0.3 wt % Zn_2GeO_4 nanorods (0.045 wt % of total weight) led to 2.5 times increase in water flux with slightly increased rejection rate. Therefore, Zn_2GeO_4nanorods are an attractive additive for the development of high flux UF composite membranes.

4. CONCLUSIONS

We have demonstrated that the nanoporous structure of the active layer of poly(ether sulfone) membranes can be effectively tailored by adding hydrophilic nanowires/nanorods in the polymer casting solution. The addition of small amounts of hydrophilic germanate nanowires/nanorods (e.g., 0.3 wt % on the basis of the weight of poly(ether sulfone)) resulted in an up to 2.5 times higher water flux without significantly increasing pore size because the hydrophilic nanowires/nanorods had strong tendency to migrate out of more hydrophobic poly(ether sulfone) in the membrane formation process, creating more nanosized pores on the active layer. Specifically, the use of short germanate nanowires/nanorods (e.g., short $Ca_2Ge_7O_{16}$ nanowires with an average length of 138.7 nm and an average diameter of 12.7 nm, and Zn_2GeO_4 nanorods with an average length of 400 nm and an average diameter of 18.7 nm) is more effective in enhancing water flux, compared with long $Ca_2Ge_7O_{16}$ nanowires with lengths of several tens to hundreds of micrometers and an average of 27.3 nm; the poly(ether sulfone) composite membranes with short $Ca_2Ge_7O_{16}$ nanowires exhibited larger pore sizes than those with Zn_2GeO_4 nanorods. Our study suggests that hydrophilic nanowires/nanorods are promising for use as additive in the fabrication of polymer ultrafiltration membranes with enhanced water permeation property.

■ ASSOCIATED CONTENT

Supporting Information

Photo of nanowires well-dispersed in solvent and SEM image of long $Ca_2Ge_7O_{16}$ nanowires after sonification (Figure S1), viscosity of casting solution with different nanowire loading (Figure S2), SEM images of top surface (Figures S3 and S4) and cross-section (Figure S5) of the pristine and composite membranes, and PEG rejection and the molecular weight cutoff of the pristine membrane and composite membranes (Figure S6). This material is available free of charge via the Internet at http://pubs.acs.org.

■ AUTHOR INFORMATION

Corresponding Author

*E-mail: huanting.wang@monash.edu. Tel.: +61399053449.

Author Contributions

The manuscript was written through contributions of all authors. All authors have given approval to the final version of the manuscript.

Notes

The authors declare no competing financial interest.

■ ACKNOWLEDGMENTS

This work is supported by the Australian Research Council (Project no. DP140101591). H.W. thanks the Australian Research Council for a Future Fellowship (Project FT100100192). The authors acknowledge technical assistance from staff at Monash Center for Electron Microscopy of Monash University.

■ REFERENCES

(1) Cho, J.; Amy, G.; Pellegrino, J. Membrane Filtration of Natural Organic Matter: Factors and Mechanisms Affecting Rejection and Flux Decline with Charged Ultrafiltration (UF) Membrane. *J. Membr. Sci.* **2000**, *164*, 89−110.

(2) McVerry, B. T.; Temple, J. A. T.; Huang, X.; Marsh, K. L.; Hoek, E. M. V.; Kaner, R. B. Fabrication of Low-Fouling Ultrafiltration Membranes Using a Hydrophilic, Self-Doping Polyaniline Additive. *Chem. Mater.* **2013**, *25*, 3597−3602.

(3) Shannon, M. A.; Bohn, P. W.; Elimelech, M.; Georgiadis, J. G.; Mariñas, B. J.; Mayes, A. M. Science and Technology for Water Purification in the Coming Decades. *Nature* **2008**, *452*, 301−310.

(4) Wang, Q.; Samitsu, S.; Ichinose, I. Ultrafiltration Membranes Composed of Highly Cross-Linked Cationic Polymer Gel: the Network Structure and Superior Separation Performance. *Adv. Mater.* **2011**, *23*, 2004−2008.

(5) Zhang, X.; Zhang, T.; Ng, J.; Sun, D. D. High-Performance Multifunctional TiO_2 Nanowire Ultrafiltration Membrane with a Hierarchical Layer Structure for Water Treatment. *Adv. Funct. Mater.* **2009**, *19*, 3731−3736.

(6) Leob, S.; Sourirajan, S. Sea Water Demineralization by Means of an Osmotic Membrane. *Adv. Chem.* **1963**, *38*, 117−132.

(7) Boom, R. M.; Wienk, I. M.; Vandenboomgaard, T.; Smolders, C. A. Microstructures in Phase Inversion Membranes. 2. the Role of a Polymeric Additive. *J. Membr. Sci.* **1992**, *73*, 277−292.
(8) Smolders, C. A.; Reuvers, A. J.; Boom, R. M.; Wienk, I. M. Microstructures in Phase-Inversion Membranes 0.1. Formation of Macrovoids. *J. Membr. Sci.* **1992**, *73*, 259−275.
(9) Young, T. H.; Chen, L. W. Pore Formation Mechanism of Membranes from Phase Inversion Process. *Desalination* **1995**, *103*, 233−247.
(10) Stropnik, C.; Germic, L.; Zerjal, B. Morphology Variety and Formation Mechanisms of Polymeric Membranes Prepared by Wet Phase Inversion. *J. Appl. Polym. Sci.* **1996**, *61*, 1821−1830.
(11) Zhao, Y. F.; Zhu, L. P.; Yi, Z.; Zhu, B. K.; Xu, Y. Y. Improving the Hydrophilicity and Fouling-resistance of Polysulfone Ultrafiltration Membranes via Surface Zwitterionicalization Mediated by Polysulfone-based Triblock Copolymer Additive. *J. Membr. Sci.* **2013**, *440*, 40−47.
(12) Majeed, S.; Fierro, D.; Buhr, K.; Wind, J.; Du, B.; Boschetti-de-Fierro, A.; Abetz, V. Multi-walled Carbon Nanotubes (MWCNTs) Mixed Polyacrylonitrile (PAN) Ultrafiltration Membranes. *J. Membr. Sci.* **2012**, *403*, 101−109.
(13) Wei, Y.; Chu, H. Q.; Dong, B. Z.; Li, X.; Xia, S. J.; Qiang, Z. M. Effect of TiO_2 Nanowire Addition on PVDF Ultrafiltration Membrane Performance. *Desalination* **2011**, *272*, 90−97.
(14) Yin, J.; Zhu, G.; Deng, B. Multi-walled carbon nanotubes (MWNTs)/polysulfone (PSU) Mixed Matrix Hollow Fiber Membranes for Enhanced Water Treatment. *J. Membr. Sci.* **2013**, *437*, 237−248.
(15) De Lannoy, C. F.; Soyer, E.; Wiesner, M. R. Optimizing Carbon Nanotube-reinforced Polysulfone Ultrafiltration membranes through Carboxylic Acid Functionalization. *J. Membr. Sci.* **2013**, *447*, 395−402.
(16) Rahimpour, A.; Jahanshahi, M.; Khalili, S.; Mollahosseini, A.; Zirepour, A.; Rajaeian, B. Novel Functionalized Carbon Nanotubes for Improving the Surface Properties and Performance of Polyethersulfone (PES) Membrane. *Desalination* **2012**, *286*, 99−107.
(17) Amirilargani, M.; Sabetghadam, A.; Mohammadi, T. Polyethersulfone/polyacrylonitrile Blend Ultrafiltration Membranes with Different Molecular Weight of Polyethylene Glycol: Preparation, Morphology and Antifouling Properties. *Polym. Adv. Technol.* **2012**, *23*, 398−407.
(18) Marchese, J.; Ponce, M.; Ochoa, N. A.; Pradanos, P.; Palacio, L.; Hernandez, A. Fouling Behaviour of Polyethersulfone UF Membranes Made with Different PVP. *J. Membr. Sci.* **2003**, *211*, 1−11.
(19) Zhao, S.; Wang, Z.; Wei, X.; Tian, X.; Wang, J.; Yang, S.; Wang, S. Comparison Study of the Effect of PVP and PANI Nanofibers Additives on Membrane Formation Mechanism, Structure and Performance. *J. Membr. Sci.* **2011**, *385*, 110−122.
(20) Wei, Y.; Chu, H. Q.; Dong, B. Z.; Li, X.; Xia, S. J.; Qiang, Z. M. Effect of TiO_2 Nanowire Addition on PVDF Ultrafiltration Membrane Performance. *Desalination* **2011**, *272*, 90−97.
(21) Celik, E.; Park, H.; Choi, H.; Choi, H. Carbon Nanotube Blended Polyethersulfone Membranes for Fouling Control in water treatment. *Water Res.* **2011**, *45*, 274−282.
(22) Li, J. F.; Xu, Z. L.; Yang, H.; Yu, L. Y.; Liu, M. Effect of TiO_2 Nanoparticles on the Surface Morphology and Performance of Microporous PES membrane. *Appl. Surf. Sci.* **2009**, *255*, 4725−4732.
(23) Fan, Z.; Wang, Z.; Sun, N.; Wang, J.; Wang, S. Performance Improvement of Polysulfone Ultrafiltration Membrane by Blending with Polyaniline Nanofibers. *J. Membr, Sci.* **2008**, *320*, 363−371.
(24) Majeed, S.; Fierro, D.; Buhr, K.; Wind, J.; Du, B.; Boschetti-de-Fierro, A.; Abetz, V. Multi-walled Carbon Nanotubes (MWCNTs) Mixed Polyacrylonitrile (PAN) Ultrafiltration Membranes. *J. Membr. Sci.* **2012**, *403*, 101−109.
(25) Li, W.; Yin, Y. X.; Xin, S.; Song, W. G.; Guo, Y. G. Low-cost and Large-scale Synthesis of Alkaline Earth Metal Germanate Nanowires as a New Class of Lithium Ion Battery Anode Material. *Energy Environ. Sci.* **2012**, *5*, 8007−8013.
(26) Liu, Q.; Zhou, Y.; Kou, J.; Chen, X.; Tian, Z.; Gao, J.; Yan, S.; Zou, Z. High-Yield Synthesis of Ultralong and Ultrathin Zn_2GeO_4 Nanoribbons toward Improved Photocatalytic Reduction of CO_2 into Renewable Hydrocarbon Fuel. *J. Am. Chem. Soc.* **2010**, *132*, 14385−14387.
(27) Wang, Y. Q.; Wang, T.; Su, Y. L.; Peng, F. B.; Wu, H.; Jiang, Z. Y. Remarkable Reduction of Irreversible Fouling and Improvement of the Permeation Properties of Poly(ether sulfone) Ultrafiltration Membranes by Blending with Pluronic F127. *Langmuir* **2005**, *21*, 11856−11862.
(28) Guillen, G. R.; Pan, Y.; Li, M.; Hoek, E. M. V. Preparation and Characterization of Membranes Formed by Nonsolvent Induced Phase Separation: A Review. *Ind. Eng. Chem. Res.* **2011**, *50*, 3798−3817.
(29) Low, Z. X.; Razmjou, A.; Wang, K.; Gary, S.; Duke, M.; Wang, H. Effect of Addition of Two-dimensional ZIF-L Nanoflakes on the Properties of Polyethersulfone Ultrafiltration Membrane. *J. Membr. Sci.* **2014**, *460*, 9−17.
(30) Dietz, P.; Hansma, P. K.; Inacker, O.; Lehmann, H. D.; Herrmann, K. H. Surface Pore Structures of Microfiltration and Ultrafiltration Membranes Imaged with the Atomic Force Microscope. *J. Membr. Sci.* **1992**, *65*, 101−111.
(31) Peeva, P. D.; Million, N.; Ulbricht, M. Factors Affecting the Sieving Behavior of Anti-Fouling Thin-layer Cross-linked Hydrogel Polyethersulfone Composite Ultrafiltration Membranes. *J. Membr. Sci.* **2012**, *390*, 99−112.